

Microscopic DC-TDHF study of heavy-ion potentials and fusion cross sections

V E Oberacker¹, A S Umar¹ and R Keser²

¹ Department of Physics and Astronomy, Vanderbilt University, Nashville, TN 37235, USA

² RTE University, Science and Arts Faculty, Department of Physics, 53100, Rize, TURKEY

E-mail: volker.e.oberacker@vanderbilt.edu

Abstract. We study heavy-ion fusion reactions at energies near the Coulomb barrier, in particular with neutron-rich radioactive ion beams. Dynamic microscopic calculations are carried out on a three-dimensional lattice using the Density-Constrained Time-Dependent Hartree-Fock (DC-TDHF) method. New results are presented for the $^{132}\text{Sn}+^{40}\text{Ca}$ system which are compared to $^{132}\text{Sn}+^{48}\text{Ca}$ studied earlier. Our theoretical fusion cross-sections agree surprisingly well with recent data measured at HRIBF. We also study the near- and sub-barrier fusion of $^{24,16}\text{O}$ on ^{12}C which is important to determine the composition and heating of the crust of accreting neutron stars.

1. Introduction

The calculation of heavy-ion interaction potentials is of fundamental importance for the study of fusion reactions between stable and neutron-rich nuclei, and for the study of superheavy element production. We have developed a fully microscopic method to extract ion-ion potentials directly from the Time-Dependent Hartree-Fock (TDHF) time-evolution of the nuclear system. The only input is the effective NN interaction (Skyrme), and there are no adjustable parameters.

Radioactive ion beam facilities have opened up the possibility to study fusion reactions of neutron-rich nuclei. In many cases, the dynamics of the neutron rich skin of these nuclei enhances the sub-barrier fusion cross section over that predicted by a simple static barrier penetration model, but in some cases suppression of fusion is also observed. Very recently, at the HRIBF facility a series of experiments has been carried out with radioactive ^{132}Sn beams on $^{40,48}\text{Ca}$ targets [1]. Also, at the GANIL-SPIRAL facility a reaccelerated beam of ^{20}O was used to measure near- and sub-barrier fusion with a ^{12}C target [2].

The time-dependent Hartree-Fock (TDHF) theory provides a useful foundation for a fully microscopic many-body theory of large amplitude collective motion [3, 4] including deep-inelastic and fusion reactions. Recently it has become feasible, for the first time, to perform TDHF calculations on a 3D Cartesian grid without any symmetry restrictions and with much more accurate numerical methods [5, 6, 7, 8, 9]. At the same time the quality of effective interactions has also been substantially improved [10, 11, 12]. During the past several years, we have developed the DC-TDHF method for calculating heavy-ion potentials [13], and we have applied this method to calculate fusion and capture cross sections above and below the barrier. So far, we have studied the systems $^{132}\text{Sn}+^{64}\text{Ni}$ [14], $^{64}\text{Ni}+^{64}\text{Ni}$, $^{16}\text{O}+^{208}\text{Pb}$ [15], $^{132,124}\text{Sn}+^{96}\text{Zr}$, and we have studied the entrance channel dynamics of hot and cold fusion reactions leading

to superheavy element $Z = 112$ [16]. Most recently, we have investigated sub-barrier fusion and pre-equilibrium giant resonance excitation between various tin + calcium isotopes [17] and calcium + calcium isotopes [18]. Last not least, we have studied sub-barrier fusion reactions between both stable and neutron-rich isotopes of oxygen and carbon [19] that occur in the neutron star crust. In all cases, we have found good agreement between the measured fusion cross sections and the DC-TDHF results. This is rather remarkable given the fact that the only input in DC-TDHF is the Skyrme effective N-N interaction, and there are no adjustable parameters.

2. Unrestricted TDHF dynamics

The TDHF equations of motion are obtained from the variational principle

$$\delta S = \delta \int_{t_1}^{t_2} dt \langle \Phi(t) | H - i\hbar \frac{\partial}{\partial t} | \Phi(t) \rangle = 0, \quad (1)$$

where H denotes the quantum many-body Hamiltonian of the system consisting of kinetic energy and Coulomb / nuclear two-body interactions. The main approximation in TDHF is that the many-body wave function $\Phi(t)$ is assumed to be a single time-dependent Slater determinant which consists of an anti-symmetrized product of single-particle wave functions

$$\Phi(r_1, \dots, r_A; t) = (A!)^{-1/2} \det|\phi_\lambda(r_i, t)|. \quad (2)$$

The variational principle confined to the subspace of Slater determinants yields the TDHF equations for the single-particle wave functions

$$h(\{\phi_\mu\}) \phi_\lambda(r, t) = i\hbar \frac{\partial}{\partial t} \phi_\lambda(r, t) \quad (\lambda = 1, \dots, A), \quad (3)$$

where $h = \partial E / \partial \rho$ denotes the mean-field Hamiltonian.

In the present TDHF calculations we use the Skyrme SLy4 interaction [10] for the nucleons including all of the time-odd terms in the mean-field Hamiltonian [5]. The numerical calculations are carried out on a 3D Cartesian lattice. For $^{40,48}\text{Ca} + ^{132}\text{Sn}$ the lattice spans 50 fm along the collision axis and 30 – 42 fm in the other two directions, depending on the impact parameter. Derivative operators on the lattice are represented by the Basis-Spline collocation method. One of the major advantages of this method is that we may use a relatively large grid spacing of 1.0 fm and nevertheless achieve high numerical accuracy. First we generate very accurate static HF wave functions for the two nuclei on the 3D grid. The static HF equations are solved with the damped gradient iteration method. The initial separation of the two nuclei is 22 fm for central collisions. In the second step, we apply a boost operator to the single-particle wave functions. The time-propagation is carried out using a Taylor series expansion (up to orders 10 – 12) of the unitary mean-field propagator, with a time step $\Delta t = 0.4$ fm/c.

In Figures 1,2,3,4 we show contour plots of the TDHF mass density for a central collision of $^{48}\text{Ca} + ^{132}\text{Sn}$ at $E_{\text{c.m.}} = 140$ MeV. The density distributions are shown as a function of time, or equivalently, as a function of the internuclear distance R .

3. DC-TDHF method: ion-ion potential and fusion cross section

In the absence of a true quantum many-body theory of barrier tunneling, sub-barrier fusion calculations are reduced to the calculation of a potential barrier between the interacting nuclei and a subsequent calculation of tunneling through the barrier [14]. To date, theoretical studies of fusion cross sections are still dominated by phenomenological methods such as the coupled-channels (CC) approach [20]. In this approach, one either uses empirical parameterizations of

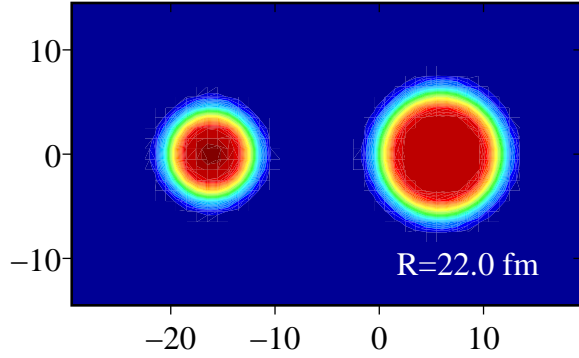


Figure 1. Central collision of $^{48}\text{Ca}+^{132}\text{Sn}$ at $E_{\text{c.m.}} = 140$ MeV. Shown is a contour plot of the TDHF mass density at internuclear distance $R = 22.0$ fm.

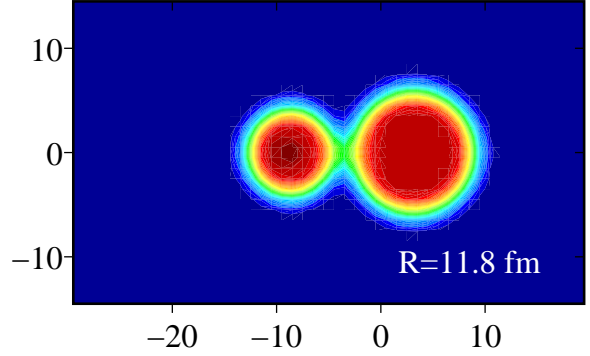


Figure 2. Mass density at $R = 11.8$ fm. A neck between the two fragments is starting to develop.

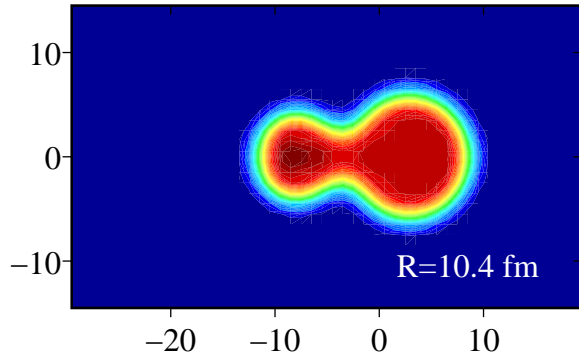


Figure 3. Mass density at $R = 10.4$ fm. The neck broadens resulting in increased mass transfer.

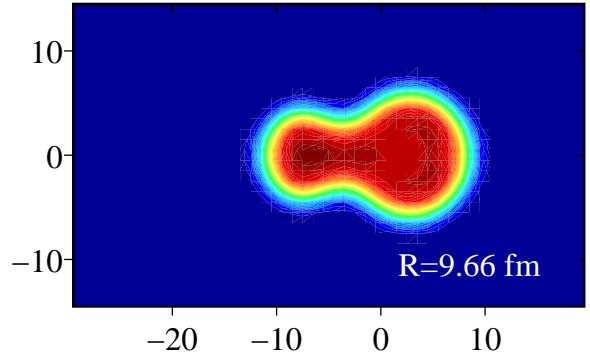


Figure 4. Mass density at $R = 9.66$ fm corresponding to the capture point.

the ion-ion potential (e.g. Woods-Saxon) or one calculates the potential with the double-folding method using experimental or theoretical nuclear densities for projectile and target. In the latter case, one relies on the “frozen density” or “sudden” approximation in which the nuclear densities are unchanged during the computation of the ion-ion potential as a function of the internuclear distance. The frozen density approximation ignores dynamical effects such as neck formation during the nuclear overlap. It has been demonstrated that for deep sub-barrier energies the inner part of the potential barrier plays a very important role [21].

While phenomenological methods provide a useful starting point for the analysis of fusion data, it is desirable to use a microscopic many-body theory. We have developed a fully microscopic method to extract heavy-ion interaction potentials $V(R)$ from the TDHF time-evolution of the dinuclear system.

In our DC-TDHF approach, the time-evolution takes place with no restrictions. At certain times t or, equivalently, at certain internuclear distances $R(t)$ the instantaneous TDHF density

$$\rho_{\text{TDHF}}(r, t) = \langle \Phi(t) | \rho | \Phi(t) \rangle \quad (4)$$

is used to perform a static Hartree-Fock energy minimization

$$\delta \langle \Phi_\rho | H - \int d^3r \lambda(r) \rho(r) | \Phi_\rho \rangle = 0 \quad (5)$$

while constraining the proton and neutron densities to be equal to the instantaneous TDHF densities

$$\langle \Phi_\rho | \rho | \Phi_\rho \rangle = \rho_{\text{TDHF}}(r, t) . \quad (6)$$

These equations determine the state vector Φ_ρ . This means we allow the single-particle wave functions to rearrange themselves in such a way that the total energy is minimized, subject to the TDHF density constraint. We have a self-organizing system which selects its path following the dynamics given by the microscopic TDHF equations.

In a typical DC-TDHF run, we utilize a few thousand time steps, and the density constraint is applied every 20 time steps. We refer to the minimized energy as the ‘‘density constrained energy’’ $E_{\text{DC}}(R)$

$$E_{\text{DC}}(R) = \langle \Phi_\rho | H | \Phi_\rho \rangle . \quad (7)$$

The ion-ion interaction potential $V(R)$ is essentially the same as $E_{\text{DC}}(R)$, except that it is renormalized by subtracting the constant binding energies E_{A_1} and E_{A_2} of the two individual nuclei

$$V(R) = E_{\text{DC}}(R) - E_{A_1} - E_{A_2} . \quad (8)$$

The interaction potentials calculated with the DC-TDHF method incorporate all of the dynamical entrance channel effects such as neck formation, particle exchange, internal excitations, and deformation effects. While the outer part of the potential barrier is largely determined by the entrance channel properties, the inner part of the potential barrier is strongly sensitive to dynamical effects such as particle transfer and neck formation.

Using TDHF dynamics, it is also possible to compute the corresponding coordinate dependent mass parameter $M(R)$ using energy conservation at zero impact parameter [15]. As expected, at large distance R the mass $M(R)$ is equal to the reduced mass μ of the system. At smaller distances, when the nuclei overlap, the mass parameter increases in all cases. Instead of solving the Schrödinger equation with coordinate dependent mass parameter $M(R)$ it is numerically advantageous to use the constant reduced mass μ and to transfer the coordinate-dependence of the mass to a scaled potential using a scale transformation (for details, see [15]). For simplicity of notation, we denote this transformed potential in the following by $V(R)$. In general, we observe that the coordinate-dependent mass changes only the interior region of the potential barriers, and this change is most pronounced at low $E_{\text{c.m.}}$ energies.

The Schrödinger equation for the coordinate R involving constant reduced mass μ and transformed potential $V(R)$ has the familiar form

$$\left[\frac{-\hbar^2}{2\mu} \frac{d^2}{dR^2} + \frac{\hbar^2 \ell(\ell+1)}{2\mu R^2} + V(R) - E_{\text{c.m.}} \right] \psi_\ell(R) = 0 . \quad (9)$$

By numerical integration of Eq. (9) using the well-established *Incoming Wave Boundary Condition* (IWBC) method we obtain the barrier penetrabilities T_ℓ which determine the total fusion cross section

$$\sigma_{\text{fus}}(E_{\text{c.m.}}) = \frac{\pi \hbar^2}{2\mu E_{\text{c.m.}}} \sum_{\ell=0}^{\infty} (2\ell+1) T_\ell(E_{\text{c.m.}}) . \quad (10)$$

4. Numerical results

In Fig. 5 we show heavy-ion interaction potentials for $^{132}\text{Sn}+^{40}\text{Ca}$ calculated with the DC-TDHF method. The potentials have been transformed so that they correspond to a constant reduced mass μ . In general, the potentials are energy-dependent and they are shown here at four different TDHF energies. Our results demonstrate that in these heavy systems the potential barrier height increases dramatically with increasing energy E_{TDHF} , and the barrier peak moves inward towards smaller R -values. Note that the potential calculated at high energy ($E_{\text{TDHF}} = 180$ MeV) has a

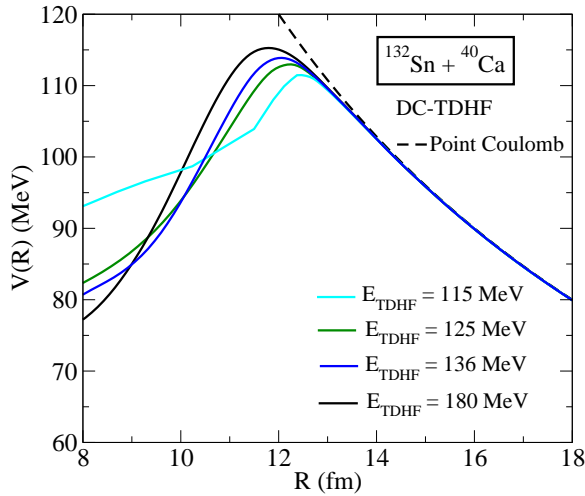


Figure 5. Transformed heavy-ion interaction potentials $V(R)$ corresponding to the reduced mass μ . The potentials show a dramatic dependence on energy.

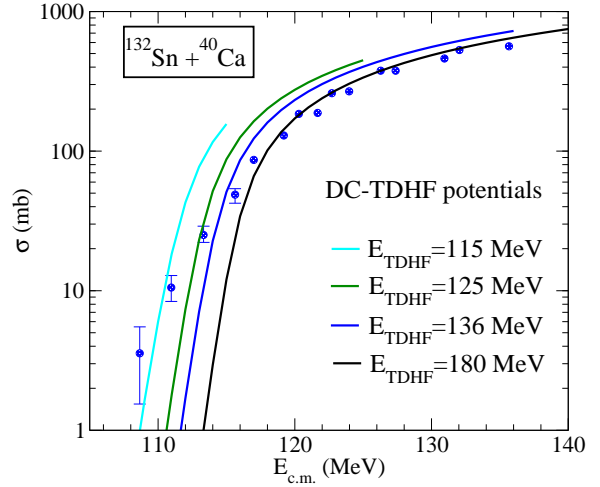


Figure 6. Total fusion cross sections obtained with the DC-TDHF method for $^{132}\text{Sn}+^{40}\text{Ca}$. The cross sections are calculated from Eq. (10) using the transformed potential $V(R)$ in Fig. 5 at four different energies. The experimental data are taken from Ref. [1].

barrier $E_B = 115.3$ MeV located at $R = 11.8$ fm, whereas the potential calculated at low energy ($E_{\text{TDHF}} = 115$ MeV) has a barrier of only $E_B = 111.5$ MeV located at $R = 12.4$ fm.

In Fig. 6 we show total fusion cross sections obtained with the DC-TDHF method for $^{132}\text{Sn}+^{40}\text{Ca}$. Also shown are experimental data obtained at HRIBF [1]. The main point of this display is to demonstrate that the energy-dependence of the heavy-ion potential is crucial for an understanding of the strong fusion enhancement at subbarrier energies. At very high energy ($E_{\text{TDHF}} = 180$ MeV) the potential approaches the limit of the frozen density approximation: the collision is so fast that the nuclei have no time to rearrange their densities. We observe that the measured fusion cross sections at energies $E_{\text{c.m.}} > 118$ MeV are well-described by this high-energy potential. At low energies, however, the situation is quite different: Due to the slow motion of the nuclei, the nuclear densities have time to rearrange resulting in neck formation, surface vibrations, particle transfer, and the interior region of the heavy-ion potential is strongly modified. These effects (which are included in TDHF) lower the fusion barrier as described above, thus strongly enhancing the subbarrier fusion cross section. We observe that the data points measured at the two lowest energies $E_{\text{c.m.}} = 108.6$ and 111 MeV can be understood by the heavy-ion potential calculated at $E_{\text{TDHF}} = 115$ MeV.

In Fig. 8 we show total fusion cross sections for $^{132}\text{Sn}+^{48}\text{Ca}$ which contains 8 additional neutrons. In this case, we have interpolated the theoretical cross sections obtained with the energy-dependent DC-TDHF potentials [17]. We can see that our theoretical cross sections agree remarkably well with the experimental data. If one compares the fusion cross sections for both systems at low energies, one finds the surprising result that fusion of ^{132}Sn with ^{40}Ca yields a larger cross section than with ^{48}Ca . For example, at $E_{\text{c.m.}} = 110$ MeV we find an experimental cross section of ≈ 6 mb for $^{132}\text{Sn}+^{40}\text{Ca}$ as compared to 0.8 mb for the more neutron-rich system $^{132}\text{Sn}+^{48}\text{Ca}$. This behavior can be understood by examining the corresponding heavy-ion potentials which are shown in Fig. 7. Both potentials have been calculated at the same center-of-mass energy $E_{\text{TDHF}} = 120$ MeV. We observe that while the barrier heights and positions for both systems are approximately the same, the *width* of the DC-TDHF potential barrier

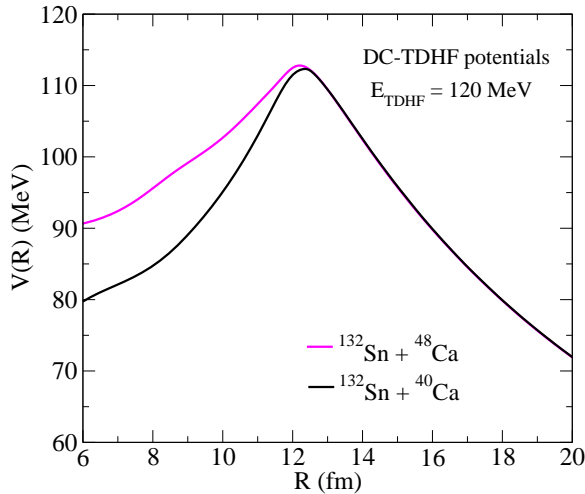


Figure 7. Transformed heavy-ion potentials $V(R)$ at low energy $E_{\text{TDHF}} = 120$ MeV for the systems $^{132}\text{Sn}+^{40,48}\text{Ca}$.

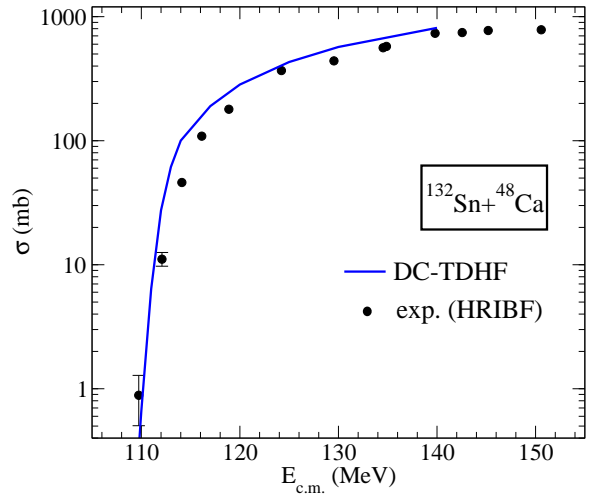


Figure 8. Total fusion cross sections obtained with the DC-TDHF method for $^{132}\text{Sn}+^{48}\text{Ca}$. The experimental data are taken from Ref. [1].

for $^{132}\text{Sn}+^{40}\text{Ca}$ is substantially smaller than for $^{132}\text{Sn}+^{48}\text{Ca}$, resulting in enhanced sub-barrier fusion at low energy.

Fusion of very neutron rich nuclei may be important to determine the composition and heating of the crust of accreting neutron stars [19]. In Fig. 9 we show the DC-TDHF potential barriers for the C+O system. The higher barrier corresponds to the $^{12}\text{C}+^{16}\text{O}$ system and has a peak energy of 7.77 MeV. The barrier for the $^{12}\text{C}+^{24}\text{O}$ system occurs at a slightly larger R value with a barrier peak of 6.64 MeV. Figure 10 shows the corresponding cross sections for the two reactions. Also shown are the experimental data from Ref. [23]. The DC-TDHF potential reproduces the experimental cross-sections quite well for the $^{12}\text{C}+^{16}\text{O}$ system, and the cross section for the neutron rich $^{12}\text{C}+^{24}\text{O}$ is predicted to be larger than that for $^{12}\text{C}+^{16}\text{O}$.

We have compared our results to the phenomenological São Paulo barrier penetration model which calculates an effective potential by folding over static densities for the projectile and target. There are interesting differences between our calculations and the São Paulo model. For the asymmetric systems $^{12}\text{C}+^{24}\text{O}$ or $^{16}\text{O}+^{24}\text{O}$ we predict an order of magnitude larger cross section than for the São Paulo model. This is likely due to dynamical effects that change the nuclear densities during the collision process caused by the rearrangement of the single-particle wave functions. This enhancement of fusion cross sections of very neutron rich nuclei can be tested in the laboratory with radioactive beams.

5. Summary and conclusions

There is mounting evidence that the TDHF equations give a good dynamical description of the early stages of low-energy heavy-ion reactions. We have developed powerful methods for extracting more information from the TDHF dynamical evolution, e.g. the ion-ion interaction potential $V(R)$, the coordinate-dependent mass parameter $M(R)$, and the dynamical excitation energy $E^*(R)$. In general, $V(R)$ depends on the center-of-mass energy and, in the case of deformed nuclei, on the Euler orientation angles. The only input is the Skyrme N-N interaction, and there are no adjustable parameters. We have calculated fusion cross sections below and above the barrier for 18 different heavy-ion systems so far. Overall, there is surprisingly good agreement with the experimental fusion data. In the future, we believe that an effort is needed

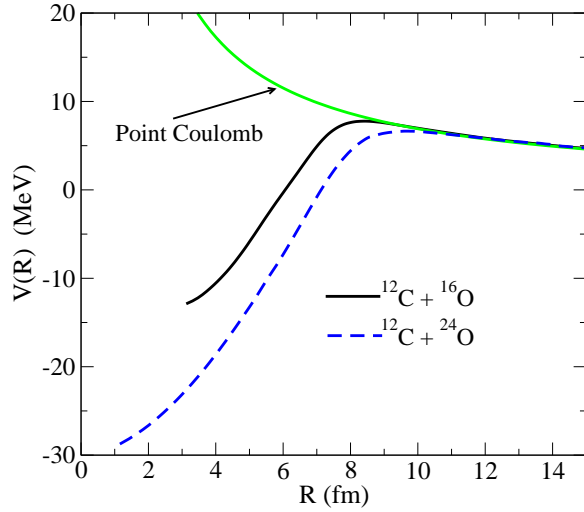


Figure 9. DC-TDHF heavy-ion potentials for the systems $^{12}\text{C}+^{16,24}\text{O}$.

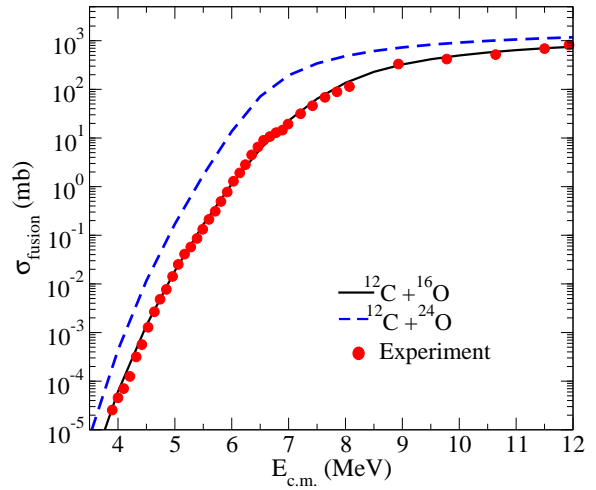


Figure 10. Total fusion cross sections versus center-of-mass energy for fusion of carbon with oxygen isotopes. The experimental data are from Ref. [23].

to incorporate deformation and scattering information into the Skyrme N-N parametrization.

Acknowledgments

This work has been supported by the U.S. Department of Energy under Grant No. DE-FG02-96ER40975 with Vanderbilt University. Some of the work presented here has been carried out in collaboration with J.A. Maruhn, P.-G. Reinhard, and C.J. Horowitz. We also acknowledge fruitful discussions with our experimental colleagues J.F. Liang, J.J. Kolata, W. Loveland and R.T. de Souza.

References

- [1] Kolata J J, Roberts A, Howard A M, Shapira D, Liang J F, Gross C J, Varner R L, Kohley Z, Villano A N, Amro H, Loveland W and Chavez E 2012 *Phys. Rev. C* **85** 054603
- [2] Rudolph M J, Gosser Z Q, Brown K, Hudan S, de Souza R T, Chbihi A, Jacquot B, Famiano M, Liang J F, Shapira D and Mercier D 2012 *Phys. Rev. C* **85** 024605
- [3] Negele J W 1982 *Rev. Mod. Phys.* **54** 913
- [4] Cusson R Y, Reinhard P G, Strayer M R, Maruhn J A and Greiner W 1985 *Z. Phys. A* **320** 475
- [5] Umar A S and Oberacker V E 2006 *Phys. Rev. C* **73** 054607
- [6] Kedziora D J and Simenel C 2010 *Phys. Rev. C* **81** 044613
- [7] Simenel C 2011 *Phys. Rev. Lett.* **106** 112502
- [8] Guo L, Maruhn J A, Reinhard P G and Hashimoto Y 2008 *Phys. Rev. C* **77**, 041301(R)
- [9] Washiyama K and Lacroix D 2008 *Phys. Rev. C* **78** 024610
- [10] Chabanat E, Bonche P, Haensel P, Meyer J and Schaeffer R 1998 *Nucl. Phys. A* **635** 231
- [11] Klüpfel P, Reinhard P G, Bürvenich T J and Maruhn J A 2009 *Phys. Rev. C* **79** 034310
- [12] Kortelainen M, Lesinski T, Moré J, Nazarewicz W, Sarich J, Schunck N, Stoitsov M V and Wild S 2010 *Phys. Rev. C* **82** 024313
- [13] Umar A S and Oberacker V E 2006 *Phys. Rev. C* **74** 021601(R)
- [14] Umar A S and Oberacker V E 2007 *Phys. Rev. C* **76** 014614
- [15] Umar A S and Oberacker V E 2009 *Eur. Phys. J. A* **39** 243
- [16] Umar A S, Oberacker V E, Maruhn J A and Reinhard P G 2010 *Phys. Rev. C* **81** 064607
- [17] Oberacker V E, Umar A S, Maruhn J A and Reinhard P G 2012 *Phys. Rev. C* **85** 034609
- [18] Keser R, Umar A S and Oberacker V E 2012 *Phys. Rev. C* **85** 044606
- [19] Umar A S, Oberacker V E and Horowitz C J 2012 *Phys. Rev. C* **85** 055801
- [20] Esbensen H, Jiang C L and Stefanini A M 2010 *Phys. Rev. C* **82** 054621

- [21] Ichikawa T, Hagino K and Iwamoto A 2007 *Phys. Rev. C* **75** 057603
- [22] Hagino K and Watanabe Y 2007 *Phys. Rev. C* **76** 021601(R)
- [23] Jiang C L, Rehm K E , Back B B and Janssens R V F 2007 *Phys. Rev. C* **75** 015803